

Determination of Stratospheric Temperature and Height Gradients From Nimbus 3 Radiation Data

GEORGE W. NICHOLAS, DALE N. HOVLAND, and ARTHUR D. BELMONT—*Research Division, Control Data Corporation, Minneapolis, Minn.*

ABSTRACT—To improve the specification of stratospheric, horizontal, temperature and geopotential height fields needed for high-flying aircraft, we derived a technique to estimate data between satellite tracks using interpolated infrared interferometer spectrometer 15- μm radiation data from Nimbus 3. The interpolation is based on the observed gradients of the medium resolution infrared 15- μm radiances between subsatellite tracks. The technique was verified with radiosonde data taken within 6 hr of the satellite data. The sample varied from 1,126 pairs at low levels to 383 pairs at 10 mb using Northern Hemisphere data for June 15–July 18, 1969. The data were separated into five latitude bands. The root-mean-square (rms) temperature differences were generally

from 2° to 5°C for all levels above 300 mb. From 500 to 300 mb, differences vary from 4° to 9°C except at high latitudes, where the differences were near 3°C. The rms differences between radiosonde heights and those calculated hydrostatically from the surface were from 30 to 280 m, increasing from the surface to 10 mb. Integration starting at 100 mb reduced the rms difference in the stratosphere to 20–120 m between 70 and 10 mb.

Comparison with operational maps at 50 and 10 mb indicates that the techniques developed here produce analyses that are in general agreement with those from radiosonde data. In addition, these techniques provide details over areas of sparse data not shown by conventional techniques.

1. INTRODUCTION

Satellite radiation observations now make it possible to derive vertical profiles of temperature on a global basis. Such data, however, are limited to points along the subsatellite tracks, which are 3000 km apart at the Equator, or to two additional points between tracks (for SIRS B). The purpose of this study is, therefore, to find a method of estimating the values at any location between tracks, thus increasing the horizontal resolution of the radiation data for the particular case of Nimbus 3 infrared interferometer spectrometer (IRIS) observations. The result is a more detailed estimate of the horizontal temperature and height gradients at each pressure level from which winds can be derived.

The IRIS on Nimbus 3 viewed only in the nadir direction, resulting in coverage only along the subsatellite track. The medium resolution infrared radiometer (MRIR) mirror, on the other hand, scanned from horizon to horizon, resulting in complete coverage between subsatellite tracks. The MRIR 15- μm channel overlapped some of the IRIS frequencies used to derive temperature profiles. The gradients of the MRIR 15- μm radiance between tracks should thus reflect, to a reasonable degree, the horizontal temperature gradients sampled at subsatellite intervals by the IRIS 15- μm spectral data at levels for which there is considerable overlap in the weighting curves (fig. 1). For the less opaque spectral intervals that are weighted heavily in the lower troposphere and whose weighting curves overlap very little with the MRIR weighting curve, the IRIS gradients correlate less with MRIR gradients. There is not complete correspondence between these gradients, of course, as many

different vertical temperature distributions can result in the same value of the MRIR 15- μm radiance. However, the research reported here was based on the premise that the atmosphere changes in a reasonably ordered manner, at least over the distances between orbits, over the time between orbits, and in the part of the atmosphere of interest (i.e., the stratosphere).

Nimbus 3 carried two experiments in which the spectral radiances in relatively narrow intervals were obtained and from which temperature profiles can be derived. One of these was the IRIS, which is described by Conrath et al. (1970) and Hanel et al. (1970). Briefly, the IRIS measures the radiances in narrow (5 cm^{-1}) spectral intervals from 400 to 2000 cm^{-1} (5–25 μm). For the research reported here, we used only two portions of the spectrum; 11 intervals within the CO_2 band at 667 cm^{-1} and the atmospheric window at 900 cm^{-1} . In addition to the spectrometers, Nimbus 3 also carried a MRIR, a five-channel scanning radiometer. It, or variations of it, has been used on meteorological satellites since TIROS 2 and has been described in the Nimbus 3 User's Guide (Goddard Space Flight Center 1969). The five wavelength regions are fairly broad. The one which concerns us here is the 645–690- cm^{-1} (15- μm) CO_2 absorption band.

2. PROCEDURES

The main purpose of this study was to develop a procedure to improve the definition of the temperature and height fields at locations away from the subsatellite tracks. A set of equivalent clear-column IRIS 15- μm radiances was determined for locations along two successive subsatellite tracks that surrounded the location for

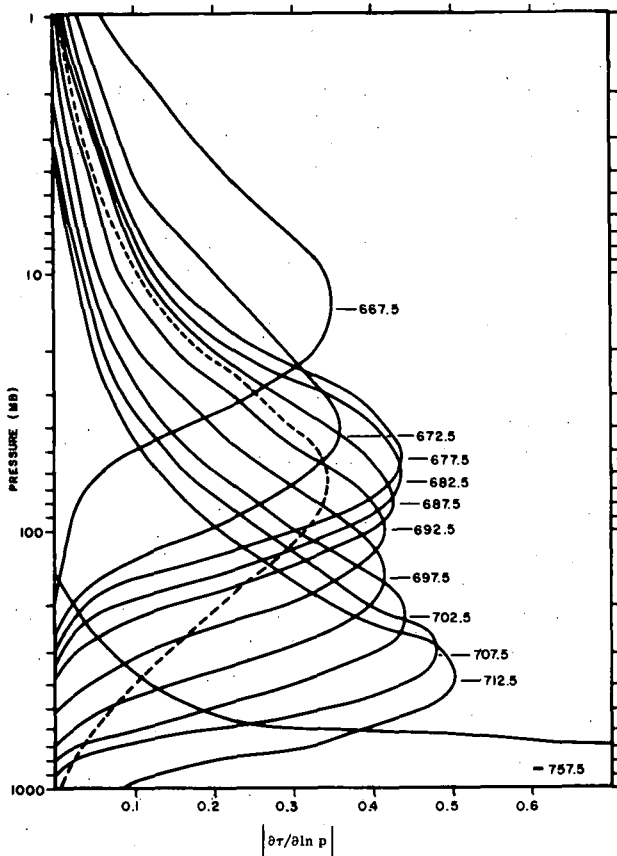


FIGURE 1.—Atmospheric weighting functions for the 667-cm⁻¹ CO₂ absorption band. The 757.5-cm⁻¹ weighting curve peaks at 1000 mb at 1.3. The MRIR 15-μm channel (645-690 cm⁻¹) is also shown (dashed line) for comparison.

which a temperature profile was desired. A regression relation was then established between gradients of the MRIR 15-μm radiance and the gradients between all combinations of locations surrounding the interpolated location for each of the 11 clear-column IRIS radiances. Based on the regression equation and weighted by distance, a set of values at the desired location was extrapolated from each set of surrounding IRIS clear-column radiances. Finally, these were reduced to an average IRIS radiance set from which the temperature and height profiles were obtained.

Clear-Column Radiances

Clouds generally exist within the field-of-view of the IRIS instrument and, hence, reduce the measured radiance for the less opaque intervals that would otherwise be measured for a cloud-free atmosphere. It is necessary to correct such cloud-contaminated measurements. The clear-column radiances were determined by the technique of Smith et al. (1970) by which the radiances were corrected for clouds, hot terrain, and high terrain.

Interpolation Method

After these corrections, the IRIS radiances were interpolated to the radiosonde locations. The computer

algorithm required at least four IRIS sets for each interpolation, of which at least one set must be from each of the two subsatellite tracks considered. Because the data were often noisy, much IRIS data had to be eliminated before interpolation.

Figure 2 shows a typical case for which a set of IRIS radiances is desired at an arbitrary, circled dot location where only the MRIR 15-μm radiance is available; both IRIS and MRIR 15-μm radiances are available at the surrounding solid dot locations. The solid dots represent locations of the IRIS data along two successive subsatellite tracks. For operational use, the circled location might be any gridpoint for which temperature and height values are desired. Here, however, the circled dot represents the location of a radiosonde, which will be used to verify the interpolation procedure. This location will be referred to as the radiosonde location or interpolated point, but it could be any arbitrary location within the confines of the two tracks. Only those data points (along the subsatellite tracks) that are less than 20° of latitude from the radiosonde location were used. Separate regression analyses were made, for each point at which interpolation was desired, to relate gradients of the IRIS and MRIR radiances between known points surrounding the interpolated point. Each regression equation was applied to determine the change of the IRIS radiance from each known point to the particular interpolated point for which the regression was calculated. At each interpolated point, a separate regression equation was calculated for each k of the 11 IRIS spectral intervals such that

$$N_x^k = a_x^k + b_x^k \frac{\partial MR_x}{\partial x} \quad (1)$$

and

$$N_y^k = a_y^k + b_y^k \frac{\partial MR_y}{\partial y}$$

Here, $k = 1, \dots, 11$, N is the change in the IRIS radiance value at the interpolated point with respect to the observed point, and $\frac{\partial MR_x}{\partial x}$ and $\frac{\partial MR_y}{\partial y}$ are the east-west and north-south components of the MRIR gradients between the known points and the interpolated point. The terms a_x and b_x are the regression coefficients for components of the radiance changes in the east-west direction, and a_y and b_y are similar coefficients for the north-south direction.

The algorithm to compute the distance-weighted, average IRIS radiance, I^k , for each spectral interval, k , then takes the form

$$I^k = \sum_{j=1}^n W_j [I_j^k + (N_x^2 + N_y^2)^{1/2}] \quad (2)$$

where n is the number of observed IRIS radiance sets, I_j^k , along the tracks, and W_j are relative weights that vary inversely as the square of the distance. The sum of W_j is one. Thus, the IRIS-measured radiances at each of the known points are adjusted by an amount that is proportional to the MRIR 15-μm radiance gradient between

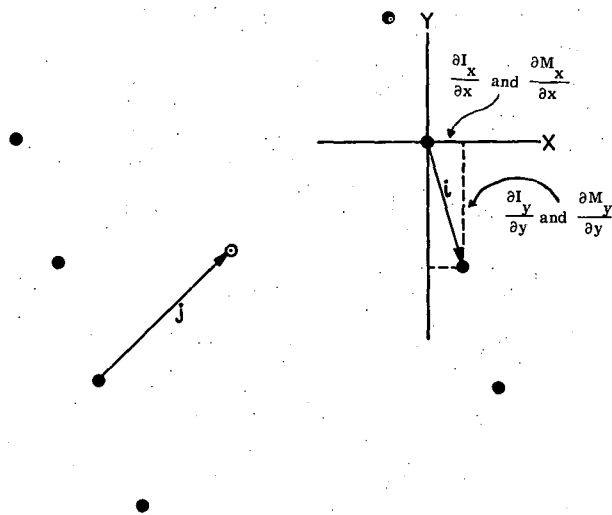


FIGURE 2.—An example of the interpolation scheme. The solid dots represent points for which both IRIS and MRIR exist. The change between these points is indicated by the subscript i . The circled dot is the location for which only MRIR is known and for which the interpolation of the surrounding IRIS is desired. Change from the known to the interpolated point is marked by a subscript j .

the known and interpolated point and to the correlation between IRIS and MRIR. An average, weighted by the inverse of the distance squared, was then taken of these adjusted IRIS values. The resulting IRIS radiance set was used to obtain the temperature profile.

The changes in the radiances from one location to another are assumed to be due to changes in temperature and not to changes in the amount and distribution of absorbing gases. For the stratosphere, this is an especially good assumption over the distances considered since only CO_2 (always considered constant), H_2O (stratosphere contains only a small amount), and O_3 (only a small amount is absorbed) are active constituents in the $15\text{-}\mu\text{m}$ spectral region.

This scheme weights the data nearest the interpolated point more heavily than more distant points and specifies the IRIS radiances between subsatellite tracks to the degree they are accounted for by the MRIR gradients. Since the less opaque spectral intervals are weighted heavily in the lower troposphere and their weighting curves overlap very little with the MRIR weighting curve, their correlation with MRIR gradients contributes little to the interpolation. In these cases, the interpolation reduces to one of almost strict space-weighted interpolation.

Derivation of Temperature and Height Profiles

The temperature profiles from the interpolated IRIS radiances were derived by a method proposed by Chahine (1968) and applied successfully by Conrath et al. (1970). The outgoing radiance at the top of the atmosphere is related to the temperature structure and absorbing gas

in the atmosphere by the radiative transfer equation,

$$I(\nu) = B[\nu, T_s(p_s)]\tau_s(\nu, p_s) - \int_{p_i}^{p_s} B[\nu, T(p)] \frac{\partial \tau(\nu, p)}{\partial \ln p} d \ln p. \quad (3)$$

The first term on the right of eq (3) is the component of radiation emitted by the surface (cloud or ground) at temperature T_s . B is the Planck radiance and τ_s is the atmospheric transmission at the surface. The second term is the contribution to the radiance by direct emission of the atmosphere. The logarithm of pressure has been chosen as the independent, height-related variable. The pressure level p_i is the top of the atmosphere above which the atmospheric contribution to the radiance is negligible. In this report, p_i is taken as 0.1 mb. The weighting function, $\partial \tau(\nu, p)/\partial(\ln p)$, is the change of transmission with change of pressure.

The second term on the right side of eq (3) is the most important term for vertical sounding, although the first term is not negligible for some spectral intervals. The first term dominates in determining the surface temperature. B and τ are both wavelength dependent. However, for any given wavelength, B is a function only of the temperature of the emitting gas, and τ is a function only of the amount or optical depth of the emitting gas. Thus, if the optical depth is known, the temperature can be directly related to the measured radiance. This is the case for CO_2 , which is uniformly mixed.

The transmittances used in this study were those reported by Smith (1969), in which he used a polynomial to fit the experimentally determined transmission values for the $15\text{-}\mu\text{m}$ CO_2 and the rotational H_2O data. Smith's tabulated regression coefficients are for 5-cm^{-1} spectral intervals. These transmittances were too large and, accordingly, for each spectral interval, the transmittance was shifted along the pressure ordinate until the radiance, computed from the radiosonde sounding, equaled the observed radiance for the corresponding spectral intervals of IRIS. A select sample of paired, cloud-free radiosonde soundings and IRIS radiance sets was used to derive these pressure adjustment factors; all computed transmittances, thereafter, were based on these factors.

Using a typical midlatitude temperature and water vapor profile, we computed the weighting curves. Those corresponding to the 5-cm^{-1} spectral intervals used in the study are shown in figure 1. In principle, the temperature can be determined from eq (3) if the radiance is known. Thus, by measuring in several spectral intervals from the strongly absorbing center (667.5 cm^{-1}) of the CO_2 band to the weakly absorbing wing of the band (757.5 cm^{-1}), we can determine several temperatures representative of different layers in the vertical, such as those shown in figure 1.

In the method used to derive temperature profiles, each level is represented by the temperature T_i ($i=1, \dots, M$) for M predetermined anchor pressure levels. Each anchor level is paired to a given spectral interval, and the

radiance associated with that level is calculated from

$$B(\nu_i, T_i^{n+1}) = \frac{\tilde{I}(\nu_i) - B(\nu_i, T_i) \tau(\nu_i, p_s)}{I^n(\nu_i) - B(\nu_i, T_s) \tau(\nu_i, p_s)} B(\nu_i, T^n) \quad (4)$$

where T_i^{n+1} is the $(n+1)$ st estimate of T_i , and $I^n(\nu_i)$ is the computed radiance from eq (3) using the n th estimate of the temperature profile, consisting of linearly interpolated temperatures between anchor levels. The measured radiances from IRIS are designated by $\tilde{I}(\nu_i)$. A first guess of a temperature profile is required to start the iterative scheme. The iteration is continued until the root-mean-square (rms) difference between the calculated and measured radiances is less than a preset value. Because the final profile is independent of the initial guess profile (Chahine 1968), the radiosonde profile was chosen as the initial guess to reduce the amount of computer time required to reach convergence.

Anchor pressure levels for this study were selected by requiring them to be at or near the level of the peaks of the weighting curves. Five July standard atmospheres (COESA 1966) representing five latitude bands were used to calculate the weighting functions. The latitude bands are 0° - 22.5° , 22.5° - 37.5° , 37.5° - 52.5° , 52.5° - 67.5° , and 67.5° - 90° . Small deviations from the weighting curve peaks were allowed in an attempt to improve the definition of the tropopause. A different set of anchor levels was used for each latitude band.

Using the calculated temperature-pressure profile and the water-vapor mixing-ratio profile from the radiosonde at the interpolation point, the radiances for the MRIR 15- μm channel were computed and compared to the average observed MRIR radiance. If the two were more than $0.01 \times 10^{-5} \text{ W}\cdot\text{cm}^{-2}\cdot\text{sr}^{-1}$ different, the temperature at each level was increased or decreased by 0.1°C , depending on the sign of the difference. This procedure was continued until the radiances agreed to within $\pm 0.01 \times 10^{-5} \text{ W}\cdot\text{cm}^{-2}\cdot\text{sr}^{-1}$. Less than 10 iterations were usually required for this criterion to be met, which means that the profile based on the interpolated IRIS radiance was changed by less than 1°C at all levels to get the measured and computed MRIR 15- μm radiances to agree. If the number of iterations reached 25, the profile was eliminated from the sample.

Once the pressure-temperature relations are derived by the iterative technique, the geopotential height can be determined from the hydrostatic equation. The height at some pressure level must be known to start the integration. For our work, the initial heights were specified from nearby radiosondes. The geostrophic wind field can be specified from the gradient of the horizontal height field determined from many temperature profiles.

3. DATA

Three types of data were used in this study: MRIR 15- μm and IRIS radiation data (both from Nimbus 3) and radiosonde data. The 34-day period for which data were analyzed was June 15-July 18, 1969. This period was dictated because it was the only one for which IRIS data were available when this study began. These data

had been reduced and formatted on tape for another requirement and were made available for this study.

It would have been more desirable to use winter data because the winter stratosphere has much larger horizontal temperature geopotential height gradients than the summer stratosphere. The IRIS of Nimbus 3 lasted only from launch on Apr. 14, to July 20, 1969, however, and there were no winter data for the Northern Hemisphere. Further, the IRIS data were noisy. No attempt was made to use only the relatively good data; however, all data were smoothed spectrally and averaged spatially during the interpolation process.

The radiosondes serve four purposes in this work. First, they provide water vapor and surface temperature information necessary to the solution of the radiative transfer equation. The surface (shelter) temperature is necessary to determine if clouds are in the field of view. Second, the radiosonde temperature profile and its vertical extrapolation above recorded levels are used as an initial guess in the iterative scheme to derive temperature profiles from the IRIS radiances. Each temperature profile was extrapolated from its highest extent to 0.1 mb by one of the five standard atmospheres cited above, depending on the latitude zone in which the sounding was located. Third, a radiosonde height provides the initial height for integrating the hydrostatic equation for IRIS-derived temperature profiles. Fourth, the radiosonde is used for verification of the derived temperature and height profiles. A more detailed description of the data processing and the special treatment of the radiosonde and IRIS data is given by Nicholas et al. (1971).

The main objective of this study was to determine the details of the horizontal temperature and geopotential height fields at stratospheric levels. One approach was to assume clouds had little or no effect on the IRIS radiances above the 100-mb level. Using the six spectral intervals of the IRIS data to which the atmosphere is most opaque, we derived the temperature profiles. The geopotential heights were found by integrating the hydrostatic equation using this derived temperature profile and starting with the radiosonde 100-mb height. In addition to the above approach, it seemed desirable to obtain heights by deriving the temperature profile starting at the surface. The surface parameters are generally defined with better resolution and are more readily available than the 100-mb data. Thus, both approaches were used throughout.

4. RESULTS

Verification Statistics

The success of the results depends on the success of both the interpolation scheme and the temperature retrievals. The latter has already been verified by Conrath et al. (1970). We therefore compare the combined interpolation and retrieval system with the radiosondes to show that the system results in reasonable values. The next section shows that, without the interpolation based on the MRIR 15- μm gradients between tracks, some details in the horizontal temperature and height gradients would not be depicted.

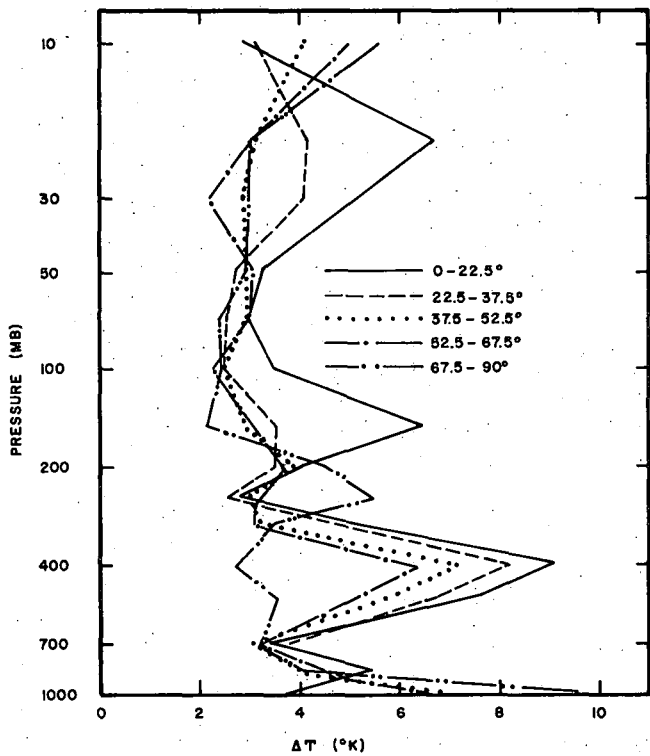


FIGURE 3.—The rms difference between interpolated, IRIS-computed temperature profiles and radiosonde temperatures for five Northern Hemisphere latitude bands.

Figure 3 displays the variation of the rms difference between the radiosonde and the interpolated, IRIS-derived temperature for five latitude bands. The rms differences were calculated and plotted at the 15 mandatory pressure levels from 1000 to 10 mb. Note that the differences are much greater in the troposphere than in the stratosphere. Except at 20 mb in the Tropics, the rms differences in the stratosphere are generally between 2° and 5°C. The 10- and 20-mb rms differences for the tropical case were based on only 7 and 23 cases, respectively, and are, therefore, probably unreliable. Except for the tropical and arctic cases, the rms differences are less than 5°C for the troposphere above 300 mb. Root-mean-square differences are large at 400 mb for all but the high-latitude case and at 1000 mb for all but the tropical case.

When the sign of the difference (radiosonde minus IRIS) at these two levels is considered, the IRIS temperature at 1000 mb is almost always higher than the radiosonde. On the other hand, the radiosonde temperature is always higher than the IRIS temperature at 400 mb. Of course, the reduction in the rms difference near 700 mb is due to this change in sign and to the fact that IRIS temperatures are determined only at these two levels and interpolated in between. There are two possible reasons for the cooler IRIS temperatures at 400 mb. First, the pressure adjustment factor used to improve the transmittance values may be underestimated for the spectral interval corresponding to the 400-mb level. This underestimation would result in computed temperature values being too low. Second, the correction technique for the cloud-contaminated radiances generally results in tem-

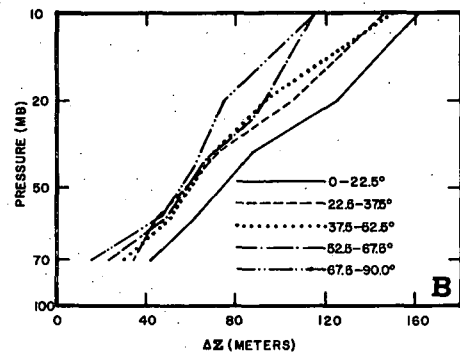
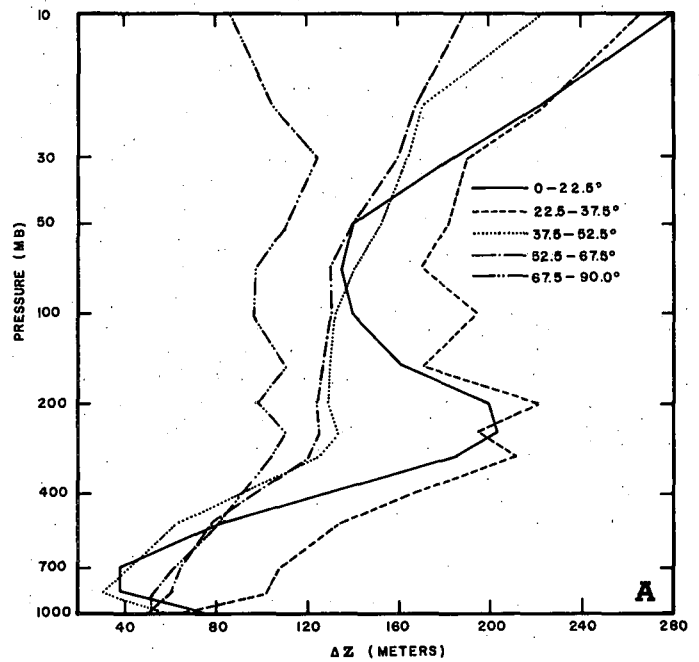


FIGURE 4.—The rms difference between interpolated, IRIS-computed, geopotential height profiles and radiosonde heights for five Northern Hemisphere latitude bands, starting the integration of the hydrostatic equation at (A) the earth's surface and (B) the 100-mb level.

perature values that are too low. Both of these causes probably contribute to the low IRIS temperature. On the other hand, the high 1000-mb temperature cannot be explained by the cloud correction method, although an erroneous pressure correction has probably resulted in an overestimation of the temperatures at this spectral interval. Another factor that may contribute to the overestimation of the 1000-mb temperature is the method used to specify the surface temperature for all surrounding IRIS sets. A method that might improve the specification of the surface temperature is one that interpolates the horizontal surface temperature field using all available surface information for the most recent observation time and then specifies the diurnal temperature change since the observation time.

Figures 4A and 4B show the rms difference in the geopotential height field. The rms differences for stratospheric levels are from about 100 to 300 m in figure 4A but are only from 20 to 160 m in figure 4B. Cumulative differences apparently occur due to the integration. Therefore, the differences are much smaller in the stratosphere

TABLE 1.—Correlations, R, between interpolated IRIS and observed radiosonde temperatures, June 15–July 20, 1969. N is sample size.

Pressure level (mb)	0–22.5°		22.5–37.5°		37.5–52.5°		52.5–67.5°		67.5–90.0°		All latitudes
	N	R	N	R	N	R	N	R	N	R	R
1000	61	0.50	161	0.38	291	0.60	186	0.65	32	0.03	0.71
850	72	.25	223	.54	522	.74	269	.73	33	.64	.77
700	74	.52	225	.51	525	.74	269	.72	33	.71	.82
500	74	.33	223	.23	521	.55	269	.47	33	.77	.68
400	74	.34	224	.36	523	.53	269	.38	33	.88	.62
300	74	.56	224	.61	523	.74	268	.57	33	.59	.80
250	51	.47	193	.68	453	.72	229	.62	19	.34	.78
200	73	.25	224	.54	525	.65	269	.78	32	.75	.67
150	73	.42	222	.72	520	.80	266	.62	33	.68	.89
100	74	.72	225	.86	525	.88	269	.67	33	.32	.96
70	72	.47	221	.66	516	.73	263	.44	33	.28	.92
50	67	.33	213	.28	497	.66	246	.42	33	.25	.87
30	64	.07	180	.14	388	.52	208	.53	27	.19	.75
20	55	.12	136	.25	323	.41	155	.50	23	.64	.64
10	36	.50	87	.22	170	.32	88	.30	7	.41	.59

TABLE 2.—Correlations between IRIS and radiosonde heights. Heights were computed from interpolated IRIS temperatures from the 100-mb height. The sample size is given in table 1.

Pressure level (mb)	Integration from surface						Integration from 100 mb					
	Latitude bands						Latitude bands					
	0°	22.5°	37.5°	52.5°	67.5°	All Lat.	0°	22.5°	37.5°	52.5°	67.5°	All Lat.
1000	0.45	0.59	0.64	0.63	0.63	0.61						
850	.67	.52	.87	.71	.59	.71						
700	.59	.51	.83	.73	.59	.73						
500	.43	.45	.81	.75	.67	.78						
400	.39	.38	.78	.73	.72	.79						
300	.31	.31	.77	.71	.74	.79						
250	.38	.41	.78	.72	.72	.83						
200	.30	.30	.77	.64	.74	.80						
150	.23	.42	.72	.57	.68	.78						
100	.10	.08	.51	.48	.62	.48						
70	.18	.13	.31	.43	.60	.35	0.84	0.94	0.97	0.97	0.98	0.96
50	.29	.11	.25	.39	.60	.49	.58	.83	.90	.90	.90	.92
30	.33	.07	.27	.41	.43	.66	.46	.66	.81	.83	.74	.90
20	.37	.11	.34	.43	.57	.74	.14	.53	.75	.75	.71	.88
10	.48	.11	.39	.43	.86	.79	.39	.43	.63	.68	.72	.87

when the integration is started at 100 mb than when the integration is begun at the surface. Because the geostrophic wind is dependent upon the horizontal gradient of the height field and not upon the absolute value of height at any level, the cumulative errors of height might be less significant than those of temperature when one estimates winds. The horizontal gradients of height are compared in the next section in the form of maps.

Table 1 shows the correlations, level by level, between the radiosonde and the IRIS-derived temperature profile. The correlation coefficients for the individual latitude bands are less than the corresponding coefficients for the case when all latitudes are included in a single data sample. This difference in correlation is a reflection of the inability of the IRIS measurements and the temperature reduction technique to specify the small-scale vertical temperature changes that are shown in the radiosonde profiles, although the large-scale temperature changes are well determined. Because the IRIS measurements were smoothed due to noise, and because the reduction technique specifies temperatures at only 11 pressure levels and intermediate levels are interpolated, the small-scale changes in the vertical are not expected to be specified as well in the IRIS as in the radiosonde temperatures.

Comparison With the National Meteorological Center Analyses

An area with good satellite data coverage and a time with relatively moderate horizontal temperature and height gradients were selected to show the operational potential of the technique to improve the description of these variables in the stratosphere. An area bounded by longitudes 50°W and 30°E and latitudes 40° and 68°N, was chosen to minimize the time difference between satellite observations and the National Meteorological Center (NMC) 1200 GMT map, which was used for comparison. Data from orbits 913, 914, and 915 on June 21, 1969, were used to construct the IRIS maps. The data from orbit 913 over this area were recorded from approximately 0943 to 0952 GMT, orbit 914 from 1130 to 1139

GMT, and orbit 915 from 1317 to 1324 GMT. Thus, data east of Greenwich were taken slightly more than 2 hr before the radiosonde data, satellite data near and just west of 0° were taken just prior to the radiosonde, and data over the western portion were taken more than 1 hr after the radiosonde.

Table 2 shows the correlation of heights for both the surface integration and the 100-mb integration of the hydrostatic equation. The correlation of the heights at levels above 100 mb is naturally much improved when the integration starts at 100 mb, rather than at the surface. The rms difference (fig. 3) of temperature shows a minimum at 100–70 mb for all latitudes, and the correlations (table 1) are greatest at these levels. These facts are significant because the MRIR 15-μm weighting curve (fig. 1) shows a maximum near these levels, indicating that the interpolation is best at those levels that contribute the most to the measured MRIR radiances.

For this application, radiosonde data were not used except to specify the 100-mb height field for determining, hydrostatically, the heights of higher levels. Because only stratospheric levels were used, surface temperature was not needed and water vapor was specified from climatology. The iteration to derive temperature profiles was initiated by using an isothermal profile of 250°K. Temperature and height profiles were computed at each intersection of a 4° longitude by 4° latitude grid for which radiation data existed.

Figure 5 is a portion of the NMC 100-mb map for this area showing the temperature and height field. The orbital tracks along which IRIS data were observed are shown for reference on this and subsequent maps. This 100-mb height field was used to determine higher level heights from the IRIS temperature profiles. The temperature field shows a warm center near 10°W, 55°N and a relatively large thermal gradient (for summer) to the southwest. Figure 6 shows the interpolated IRIS temperature field at the same 100-mb level. The warm center and the

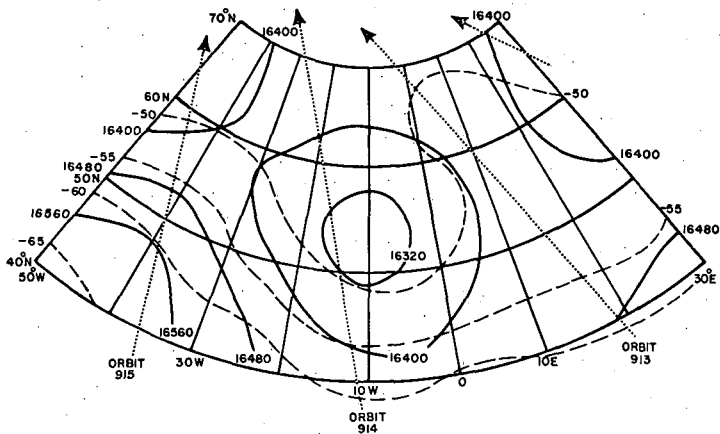


FIGURE 5.—Portion of the NMC 100-mb map for 1200 GMT, June 21, 1969. The solid lines are geopotential heights (m), and the dashed lines are temperatures ($^{\circ}\text{C}$).

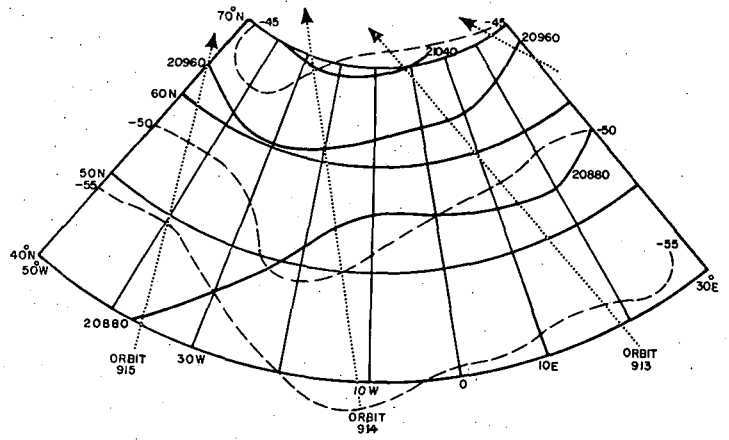


FIGURE 7.—Same as figure 5 for 50 mb.

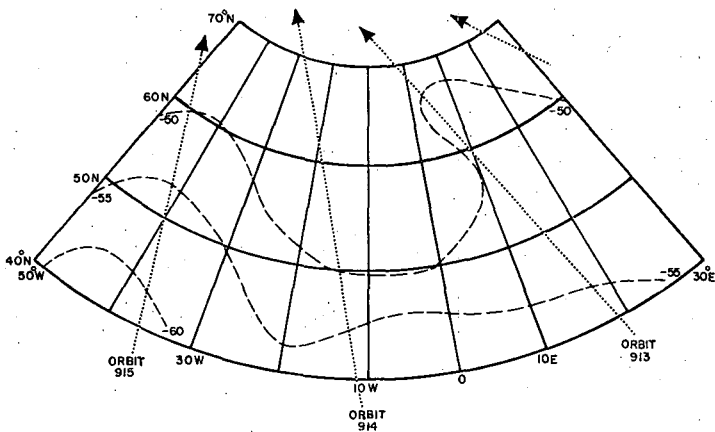


FIGURE 6.—The 100-mb temperatures derived from interpolated IRIS. The data were acquired from the orbits 913 (0943–1952 GMT), 914 (1130–1139 GMT), and 915 (1317–1324 GMT).

strong gradient are well defined; in fact, both the pattern and absolute values of the isotherms agree with the NMC analysis over the entire map. Note in particular, that, in the eastern extreme of the warm center the interpolated IRIS data is in complete agreement with the dense western European radiosonde data. Obviously, the detail in the gradient shown here would have been lost if only linear interpolation of the temperature values along the tracks between orbits 913 and 914 had been made. The IRIS interpolation indicates a warm trough in the -55°C isotherm along 20°W for which no radiosonde data were available. This thermal trough is not shown in figure 5, but it is evident in the -65°C isotherm at 33°W and 33°N (outside the border of the reproduced NMC map).

Figures 7 and 8 show, respectively, the NMC and the IRIS temperature and height analyses for 50 mb. The warm trough in both figures is in good agreement, although the IRIS -50°C trough is about 10° east of the NMC trough. The NMC position is supported by sparse ocean station data; therefore, the difference is not readily explainable. The IRIS map defines the feature well, and the magnitudes of the isotherms agree. Although not shown on the NMC analysis, the northward bending of the -55°C

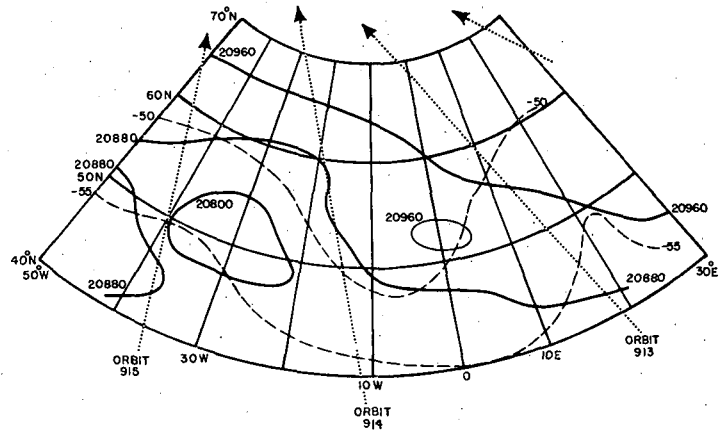


FIGURE 8.—The 50-mb temperatures (dashed line) and heights (solid line) derived from interpolated IRIS.

IRIS isotherm at 20°E can be justified by radiosonde data. The greater smoothing used in NMC procedures may explain this difference in the analyses. It is interesting that the radiation data supported an analysis that the conventional technique ignored. Again, if only spatial interpolation from one subsatellite track to the next had been used, this feature would have been missing on the IRIS analysis also. The IRIS map does not show the -45°C isotherm that appears on the northern boundary of the NMC map because no radiation data were available for the region on this day.

The temperature fields in figures 9 and 10 for the 10-mb level do not compare as favorably as for the 50-mb map. The NMC map shows the -30°C warm tongue west of that on the IRIS map. Inspection of the radiosonde data shows extremely different temperatures in this area, such as -26°C adjoining -43°C . The IRIS analysis appears as justifiable as the NMC analysis in this instance, considering the number and variance of the few reports available. The IRIS map also shows more detail than the NMC map.

The NMC automatic analysis employs extensive smoothing with an initial scan over five NMC gridpoints, even where data are plentiful. In addition, the NMC analysis may not detect such small-scale features as the Low center at 30°W on the IRIS 50-mb map over this part

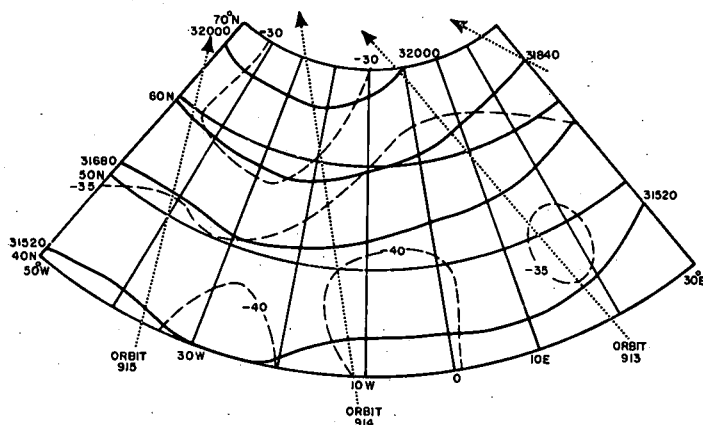


FIGURE 9.—Same as figure 5 for 10 mb.

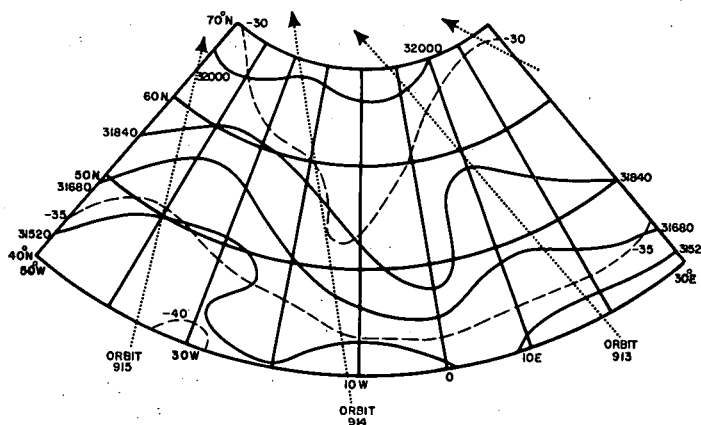


FIGURE 10.—Same as figure 8 for 10 mb.

of the ocean, where there may be only two or three radiosonde stations. The practice of extrapolating radiosonde data vertically when they do not reach these levels also contributes to the uncertainties in the NMC analyses, especially at 10 mb. In addition, 10-mb radiosonde heights at neighboring stations only a few hundred kilometers apart frequently differ by 100 m and sometimes even 200 m. The standard deviations determined from the radiosonde data for heights at 50 and 10 mb are 121 and 258 m, respectively; while, for the IRIS heights, the standard deviations are 105 and 270 m, respectively. Although the agreement at 50 and 10 mb in the height field is not good, the uncertainties in the IRIS values are probably no greater than those of the radiosondes at these levels.

It therefore appears possible, at least for summer data, that the interpolated radiation data can provide more detailed information than that which can be derived from NMC data with a reliability equal to that of the NMC product. It is paradoxical, however, that the thermal fields from independent data appear to agree better than the height fields, which are based on a common 100-mb base.

Sources of Error

Many factors can contribute to errors and uncertainties in the temperature and geopotential height profiles derived by the procedures used in this study. Some of them are:

1. Cloud-contaminated radiances.
2. Noise in the IRIS data. Severe smoothing, applied to eliminate extremes from occurring, also eliminated any large, true signals.
3. Time differences (up to ± 6 hr) between the observations of radiosonde and radiation data. Time and space differences also introduce errors in the method used to specify the surface temperature and the subsequent correction for cloud-contaminated IRIS radiances.
4. The many approximations in the solution of the radiative transfer equation and the iterative technique to derive temperature profiles. These include the uncertainty in the absorption coefficient of CO_2 for the 15- μm band, the specification of the anchor pressure levels for temperature profiles, and interpolation between anchor levels.
5. Inadequate sample size in determining the regressions.
6. Errors in the radiosonde temperatures themselves.

5. SUMMARY AND CONCLUSIONS

To improve the specification of stratospheric, horizontal temperature and geopotential height fields from subsatellite radiation data, we devised an interpolation technique to obtain estimated values of IRIS 15- μm data between subsatellite tracks. The interpolation is based on the linear regression of the IRIS and MRIR 15- μm radiance gradients between points along the tracks for which both are available. The regression equation is then applied to locations away from the track where only the MRIR data exist. A set of IRIS 15- μm radiances is specified by the interpolation, and temperature and height profiles can then be derived.

This technique was verified by interpolating at radiosonde locations and ignoring up to 6-hr time differences between radiosonde and radiation observations. The sample varied from 1,126 pairs at lower levels to 383 pairs at 10 mb, using Northern Hemisphere data for June 15–July 18, 1969. The data were analyzed separately for each of five latitude bands.

The rms differences of the radiosonde and IRIS-derived temperatures were generally between 2° and 5°C for all levels above 300 mb. For levels below 300 mb, the rms difference was as high as 9.6°C at 1000 mb for the high-latitude case. The IRIS temperature was consistently higher than the radiosonde at 1000 mb, but lower at 400 mb. Generally, the radiosonde temperatures are higher than the IRIS temperatures above 100 mb. At 50 mb, the radiosonde temperature was approximately 2°C higher for all latitudes, and the difference decreases upward. At high latitudes, the IRIS temperature was nearly 4°C higher than the radiosonde temperature at 10 mb.

The rms difference of the radiosonde and IRIS heights ranges from 30 to 280 m, generally increasing from the surface to 10 mb when the hydrostatic equation was integrated from the surface to 10 mb. Starting the integration at 100 mb (above the cloud level) resulted in lower rms differences, ranging from 20 to 120 m from 70 to 10 mb.

The horizontal gradients of temperature derived by this method compared favorably with the gradients

from NMC computer analyses (based on radiosondes) for a limited area at the 100, 50, and 10-mb levels. Ordinary spatial interpolation between tracks of the IRIS temperatures resulted in the loss of detail. The height field derived from the IRIS temperature profiles probably has no more uncertainty than radiosonde heights at those levels.

It can be concluded from this study that the MRIR-interpolated, IRIS-derived temperature and height profiles can be determined accurately enough to improve temperature gradient analyses at stratospheric levels between satellite tracks. Although it could benefit from a reduction in contributory errors, this technique can be a useful operational tool.

ACKNOWLEDGMENTS

This research was sponsored under Contract NAS8-25949 with NASA, George C. Marshall Space Flight Center. The authors are grateful to Barney Conrath of NASA, Goddard Space Flight Center, who provided the computational procedures to derive the temperature profiles.

REFERENCES

Chahine, Moustafa T., "Determination of the Temperature Profile in an Atmosphere From its Outgoing Radiance," *Journal of the*

Optical Society of America, Vol. 58, No. 12, Dec. 1968, pp. 1634-1637.

COESA, U.S. Committee on Extension to the Standard Atmosphere, *U.S. Standard Atmosphere Supplements, 1966*, U.S. Government Printing Office, Washington, D.C., 1966, 289 pp.

Conrath, Barney J., Hanel, R. A., Kunde, V. G., and Prabhakara, C., "The Infrared Interferometer Experiment on Nimbus 3," *Journal of Geophysical Research*, Vol. 75, No. 30, Oct. 1970, pp. 5831-5857.

Goddard Space Flight Center, NASA, *Nimbus III User's Guide*, National Aeronautics and Space Administration, Greenbelt, Md., 1969, 238 pp.

Hanel, Rudolf, Schlachman, B., Clark, F. D., Prokesh, C. H., Taylor, J. B., Nelson, W. M., and Chaney, L., "Nimbus III Michaelson Interferometer," *Applied Optics*, Vol. 9, No. 8, Aug. 1970, pp. 1767-1774.

Nicholas, George W., Hovland, D. N., and Belmont, A. D., "Determination of Stratospheric Temperature and Height Gradients from Nimbus III Radiation Data," *Final Report*, Contract NAS8-25949, Research Division, Control Data Corporation, Minneapolis, Minn., July 1971, 42 pp; NASA CR-1942, Nov. 1971, 61 pp.

Smith, William L., "A Polynomial Representation of Carbon Dioxide and Water Vapor Transmission," *ESSA Technical Report NESC-47*, U.S. Department of Commerce, National Environmental Satellite Center, Washington, D.C., Feb 1969, 20 pp.

Smith, William L., Woolf, H. M., and Jacob, W. J., "A Regression Method for Obtaining Real-Time Temperature and Geopotential Height Profiles From Satellite Spectrometer Measurements and its Application to Nimbus 3 'SIRS' Observations," *Monthly Weather Review*, Vol. 98, No. 8, Aug. 1970, pp. 582-603.

[Received September 27, 1971; revised August 18, 1972]